

# Journal of Materials Chemistry C

Accepted Manuscript



This article can be cited before page numbers have been issued, to do this please use: N. Natarajan, L. Shi, H. Xiao, J. Wang, L. Zhang, X. Zhang and Z. Chen, *J. Mater. Chem. C*, 2018, DOI: 10.1039/C8TC03270J.



This is an Accepted Manuscript, which has been through the Royal Society of Chemistry peer review process and has been accepted for publication.

Accepted Manuscripts are published online shortly after acceptance, before technical editing, formatting and proof reading. Using this free service, authors can make their results available to the community, in citable form, before we publish the edited article. We will replace this Accepted Manuscript with the edited and formatted Advance Article as soon as it is available.

You can find more information about Accepted Manuscripts in the [author guidelines](#).

Please note that technical editing may introduce minor changes to the text and/or graphics, which may alter content. The journal's standard [Terms & Conditions](#) and the ethical guidelines, outlined in our [author and reviewer resource centre](#), still apply. In no event shall the Royal Society of Chemistry be held responsible for any errors or omissions in this Accepted Manuscript or any consequences arising from the use of any information it contains.



## Journal Name

## ARTICLE

## Using Phosphorescent PtAu<sub>3</sub> Clusters for Superior Solution-Processable Organic Light Emitting Diodes with Very Small Efficiency Roll-Off

Received 00th January 20xx,  
Accepted 00th January 20xx

DOI: 10.1039/x0xx00000x

www.rsc.org/

Nagarajan Natarajan, Lin-Xi Shi, Hui Xiao, Jin-Yun Wang, Li-Yi Zhang, Xu Zhang,\* Zhong-Ning Chen\*

A family of highly phosphorescent PtM<sub>3</sub> (M = Au, Ag) aromatic acetylide cluster complexes supported with tetraphosphine and stabilized by  $\mu$ -chloride were synthesized by the use of weakly luminescent mononuclear Pt(PPh<sub>3</sub>)<sub>2</sub>(C≡CR)<sub>2</sub> (R = aryl) as precursors. The formation of PtM<sub>3</sub> cluster complexes involves the abstraction of chloride from dichloromethane. The dramatic difference between PtAg<sub>3</sub> and PtAu<sub>3</sub> cluster structures arises from the location of Pt atom, which is at the center of triangle-planar PtM<sub>3</sub> cluster for M = Ag whereas at one of the three corners in the PtM<sub>3</sub> triangle plane for M = Au. Perturbation of chloride ion in complexation by using halide-abstracting agent results in the formation of PtM<sub>2</sub> heterotrinnuclear structures as demonstrated by X-ray crystallography. The PtAu<sub>3</sub> complexes display intense phosphorescence with quantum yields over 90% in doped films. High-efficiency OLEDs based on PtAu<sub>3</sub> complexes were attained with external quantum efficiency (EQE) over 18%. Most importantly, the optimized devices exhibit extremely small efficiency roll-off (less than 1%) at a practical brightness over 1000 cd m<sup>-2</sup>, which is one of the best performances for solution-processable phosphorescent OLEDs.

### Introduction

Highly phosphorescent metal complexes continue to receive a great deal of attention because of their useful photophysical properties that lead to develop high-efficiency organic light emitting diodes (OLEDs).<sup>1</sup> Notably, most of highly efficient phosphorescent emitters reported so far suffer from severe efficiency roll-off at high current density or practical luminance over 1000 cd m<sup>-2</sup>, which is the main hurdle to satisfy stable high-performance OLEDs. The efficiency roll-off stems mainly from long excited-state lifetimes of the emitters leading to triplet – triplet annihilation (TTA) and triplet–charge annihilation (TCA).<sup>2</sup> Several strategies have been proposed to overcome this issue, including the design of emitters with short-lived triplet excited state,<sup>3</sup> broadening the recombination zone,<sup>4</sup> doping the emitters with large dendrons,<sup>5</sup> reducing intermolecular aggregation, and developing bipolar host materials.<sup>6–8</sup> Undoubtedly, more design strategies to attain a small efficiency roll-off remain to be established.

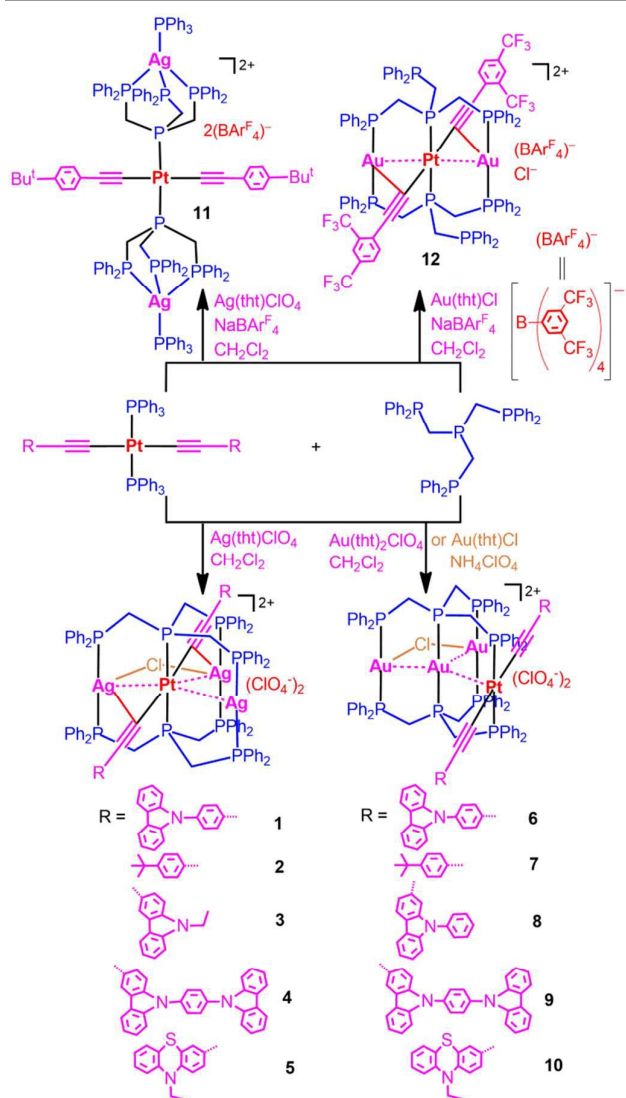
Among various available phosphorescent emitters, metal cluster complexes are of particular interest because of their

mild preparative condition, high luminescent quantum yield, good resistant to thermal and chemical degradation, and favorable solubility in organic solvents, making them as excellent candidates for efficient solution-processable OLEDs.<sup>9–21</sup> Except for the lower volatility, phosphorescent polynuclear metal cluster complexes display several advantages over mononuclear complexes, such as (i) better molecular rigidity due to the formation of polynuclear aggregates and thus more intense phosphorescence, (ii) more convenience for the regulation of emissive energy and colors by modifying both bridging and ancillary ligands, and (iii) more diverse phosphorescent characteristics owing to the participation of multiple metal ions and the formation of intermetallic interaction.

Many square-planar mononuclear platinum(II) complexes are non-luminescent or weakly emissive at room temperature, but their corresponding Pt<sup>II</sup>–M<sup>I</sup> (M = Ag, Au) heteronuclear cluster complexes become highly phosphorescent because of the much enhanced molecular rigidity upon the formation of aggregate structures.<sup>20–26</sup> For instance, mononuclear precursors Pt(PPh<sub>3</sub>)<sub>2</sub>(C≡CR)<sub>2</sub> (R = alkyl or aryl) are weakly luminescent at ambient temperature, but intense phosphorescence is frequently achieved when Pt(PPh<sub>3</sub>)<sub>2</sub>(C≡CR)<sub>2</sub> react with M<sup>+</sup> and PhP(CH<sub>2</sub>PPh<sub>2</sub>)<sub>2</sub> (dpmp) or (Ph<sub>2</sub>PCH<sub>2</sub>PCH<sub>2</sub>)<sub>2</sub> (dpmppe) to produce PtM<sub>2</sub> heterotrinnuclear entities through the substitution of PPh<sub>3</sub>.<sup>20–22</sup> The Pt<sup>II</sup>–M<sup>I</sup> intermetallic interactions play a crucial role in determining phosphorescent characteristics as well as improving molecular rigidity to achieve highly efficient phosphorescence in these PtM<sub>2</sub> complexes.

State Key Laboratory of Structural Chemistry, Fujian Institute of Research on the Structure of Matter, Chinese Academy of Sciences, Fuzhou, Fujian 350002, China  
E-mail: czn@fjirsm.ac.cn; zhangxu@fjirsm.ac.cn

† Electronic Supplementary Information (ESI) available: Experimental; details of X-ray crystallographic; computational studies and OLED device fabrication. For ESI and crystallographic data in CIF (CCDC 1846539–1846542) or other electronic format see DOI: 10.1039/x0xx00000x



Scheme 1 Synthetic Route to PtM<sub>3</sub> and PtM<sub>2</sub> (M = Ag or Au) Complexes.

Since tetraphosphine P(CH<sub>2</sub>PPh<sub>2</sub>)<sub>3</sub> (tdpmp) as a bulkier supporting ligand than triphosphine PhP(CH<sub>2</sub>PPh<sub>2</sub>)<sub>2</sub> (dpmp) could afford Pt–M cluster aggregates with higher nuclearity, better molecular rigidity and larger steric effect, it is likely that the efficiency roll-off in devices can be more effectively restrained because of the much reduced intermolecular aggregation. As expected, high-efficiency solution-processed OLEDs based on tetraphosphine-supported PtAu<sub>3</sub> cluster complexes were successfully achieved with the peak CE of 62.8 cd A<sup>-1</sup> and EQE of 18.1%. The devices display extremely low efficiency roll-off (less than 1%) at a practical luminance over 1000 cd m<sup>-2</sup>. The much lower efficiency roll-off is also ascribed to the lower doping concentration in emitting layers for PtAu<sub>3</sub> cluster complexes (3 wt%) than that for dpmp-supported PtAu<sub>2</sub> complexes (8 wt%).<sup>20,21</sup>

## Results and Discussion

### Synthesis and Characterization

The preparation of PtM<sub>3</sub> heterotetranuclear cluster complexes (Scheme 1) was carried out using the branched C<sub>3</sub> symmetrical tris(diphenylphosphinomethyl)phosphine (tdpmp) as the supporting ligand. Thus, the reactions of Pt(PPh<sub>3</sub>)<sub>2</sub>(C≡CR)<sub>2</sub>, tdpmp and Ag(tht)ClO<sub>4</sub> in 1 : 2 : 3 molar ratio expectedly gave PtAg<sub>3</sub> heterometallic cluster complexes 1–5. The products were then purified by chromatography on silica gel columns using CH<sub>2</sub>Cl<sub>2</sub>–MeOH (v/v = 20 : 1) as the eluent to give pure solids in good yields (72–84%). These compounds were satisfactorily characterized by HRMS (ESI), <sup>1</sup>H and <sup>31</sup>P[<sup>1</sup>H] NMR spectroscopy. Initially, the peaks observed from the <sup>31</sup>P[<sup>1</sup>H] NMR spectrum of PtAg<sub>3</sub> complex 1 (Figure 1a) were somewhat puzzling. We expected two sets of peaks corresponding to the P atoms bound to Pt and Ag centers, respectively. But we observed three sets of signals centered at 18.0 to 19.3 ppm, 9.0 to 9.6 ppm, and –0.6 to –4.0 ppm in 1 : 1 : 2 ratio, corresponding to 2P, 2P and 4P donors, respectively. The first multiplets with satellite peaks (Figure 1a, signal a) arise from the central P donor of P(CH<sub>2</sub>PPh<sub>2</sub>)<sub>3</sub> bonded to the Pt(II) center. The third set of signals (Figure 1a, signal c) is ascribed to two terminal P donors bound to two Ag(I) centers bridged by μ-Cl atom, whereas the second group of signals (Figure 1a, signal b) is due to the third terminal P donor bound to another Ag(I) center. The occurrence of two groups of phosphorus signals for each equivalent P atom arises from fluxional structures of PtAg<sub>3</sub> complexes due to the labile Ag–C<sub>acetylide</sub> or/and Ag–Cl bonds in fluid solutions as demonstrated previously.<sup>21a,23,27</sup>

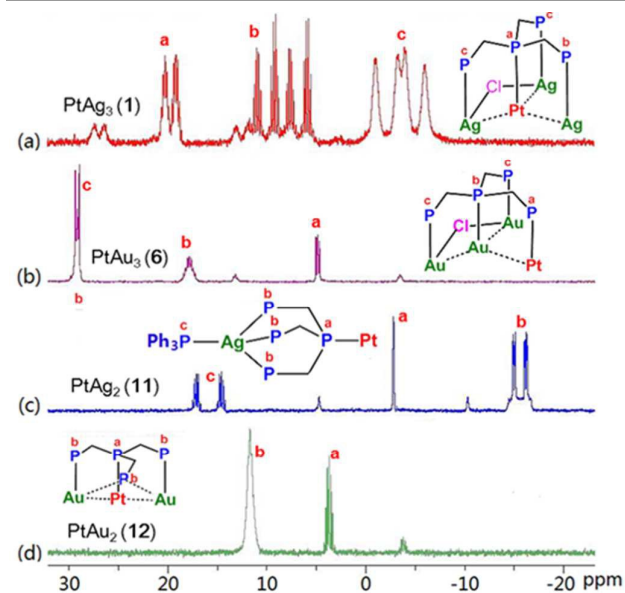


Fig 1 The <sup>31</sup>P[<sup>1</sup>H] NMR spectra of compounds 1 (a), 6 (b), 11 (c) and 12 (d) at 293 K.

Then, the structure of PtAg<sub>3</sub> complex 3 was determined by single crystal X-ray diffraction. As depicted in Figure 2a, the structure of PtAg<sub>3</sub> complex shows that two Ag atoms are bridged by a chloride ion, which matches well with the <sup>31</sup>P[<sup>1</sup>H] NMR spectral data. Obviously, the abstraction of chloride from CH<sub>2</sub>Cl<sub>2</sub> provides a source of bridging chloride atom. Such a

phenomena has already been observed in some silver(I),<sup>28</sup> copper(I)<sup>29</sup> and nickel(II)<sup>30</sup> complexes. The cationic PtAg<sub>3</sub> cluster structure is supported by dual bridging tdpmp. Of the four P donors in tetraphosphine, three terminal ones are bound to Ag(I) centers whereas the central one is bonded to platinum(II) center. All the metal atoms in PtAg<sub>3</sub> cluster lie in the same plane, in which three Ag atoms occupy the corners of an approximate isosceles triangle and the Pt atom is located in the center. The Pt–Ag distances (2.8862(7) to 3.0635(9) Å) are much shorter than the sum of van der Waals radii of platinum and silver atoms (3.4 Å), implying a significant intermetallic interaction.<sup>22,23</sup> The Ag–Ag separations, however, are longer than 4.0 Å, which precludes the possibility of intermetallic contact. Noticeably, the distance of Pt1–Ag1 (2.8862(7) Å) is obviously shorter than those of Pt1–Ag2 (3.0618(8) Å) and Pt1–Ag3 (3.0635(9) Å) as a result of Ag2 and Ag3 linked by a chloride ion ( $d_{\text{Ag2-Cl}} = 2.6373(16)$  Å and  $d_{\text{Ag3-Cl}} = 2.6086(16)$  Å). The distinct asymmetry in PtAg<sub>3</sub> cluster core is due to the constraint from Ag2–(μ-Cl)–Ag3 bridging array, which results in the much smaller angle of Ag2–Pt1–Ag3 (83.491(16)°) than those of Ag1–Pt1–Ag2 (149.156(18)°) and Ag1–Pt1–Ag3 (127.340(19)°). The Pt center is located at distorted square-planar environment composed of C<sub>2</sub>P<sub>2</sub> chromophore. Ag1 is coordinated to two P donors with P–Ag–P angle of 164.78(6)°, whereas μ-Cl bridged Ag2 and Ag3 display severely distorted tetrahedral geometry composed of CCIP<sub>2</sub> donors with the bite angles of 82.41(11)–155.14(5)°.

PtAu<sub>3</sub> complexes **6–10** (Scheme 1) were prepared by the reactions of Pt(PPh<sub>3</sub>)<sub>2</sub>(C≡CR)<sub>2</sub> with two equiv. tdpmp and three equiv. Au(tht)Cl in the presence of three equiv. NH<sub>4</sub>ClO<sub>4</sub>. Interestingly, the structures of PtAu<sub>3</sub> complexes (Figure 2b) showed dramatic variation in comparison with PtAg<sub>3</sub> complexes (Figure 2a). In strikingly contrast to PtAg<sub>3</sub> structures with Pt center bound to the central P donor of tdpmp, the Pt center in PtAu<sub>3</sub> complexes is bonded to one of the three terminal P donors while the central and other two terminal P donors of tdpmp are bound to three Au centers, respectively. The <sup>31</sup>P{<sup>1</sup>H} NMR spectra of PtAu<sub>3</sub> complexes (Figure 1b for complex **6**) exhibited three groups of signals centered at ca. 4.2–6.2, 17.8–22.7 and 29.1–30.4 ppm. The first set of signals (Figure 1b, a) with satellite peaks ( $J_{\text{Pt-P}} = 2696\text{--}2706$  Hz) are ascribed to one terminal P donor of tdpmp bound to the Pt(II) center, whereas the second one (Figure 1b, b) to the central P donor and the later triplet (Figure 1b, c) to the other two terminal P donors bonded to Au(I) centers.

As revealed by X-ray crystallography, the structure of PtAu<sub>3</sub> complex **6** (Figure 2b) indicates that acetylides are only bonded to Pt center and there are no acetylide–Au linkages observed in PtAg<sub>3</sub> complexes (Figure 2a). The PtAu<sub>3</sub> cluster atoms is on the same triangle plane, in which Au1 is located at the center, and Pt1, Au2 and Au3 at the three apexes with Pt1–Au1–Au2, Pt1–Au1–Au3 and Au2–Au1–Au3 angles of 127.15(4), 122.34(3) and 110.51(3)°, respectively. Notably, the two Au (Au2 and Au3) atoms at triangle apexes are linked by a bridging chloride, which was also observed even if [Au(tht)<sub>2</sub>]ClO<sub>4</sub> instead of Au(tht)Cl was used as the starting precursor.

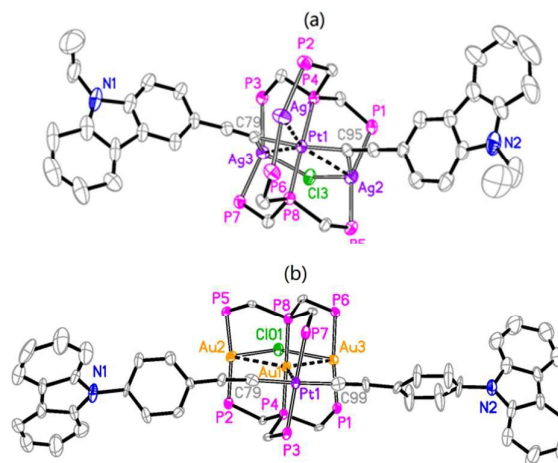


Fig 2 Perspective views of cationic PtAg<sub>3</sub> complex **3** (a) and PtAu<sub>3</sub> complex **6** (b) with 30% thermal ellipsoids. Phenyl rings of the phosphorus atoms are omitted for clarity.

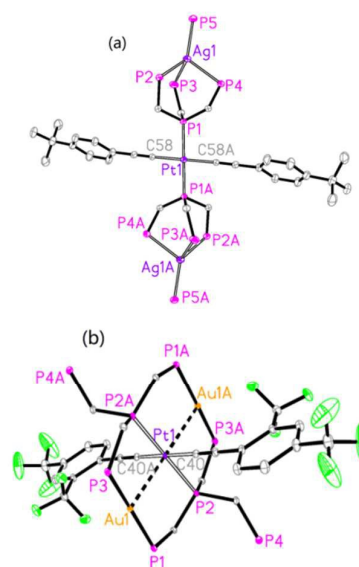


Fig 3 Perspective views of cationic PtAg<sub>2</sub> complex **11** (a) and PtAu<sub>2</sub> complex **12** (b) with 30% thermal ellipsoids. Phenyl rings of the phosphorus atoms are omitted for clarity.

The Pt center displays a square-planar coordination environment composed of trans-oriented P<sub>2</sub>C<sub>2</sub> donors. Au1 center is bound to two linearly arranged P donors with P4–Au1–P8 angle of 179.52(14)°, while Au2 and Au3 centers, exhibit T-type coordination geometry composed of P<sub>2</sub>Cl donors with P2–Au2–P5 and P1–Au3–P6 angles of 172.87(13) and 168.79(13)°, respectively. The Pt1–Au1 distance (2.9619(10) Å) is much shorter than the sum of van der Waals radii of platinum and gold atoms (3.38 Å), suggesting a significant intermetallic contact.<sup>20,21</sup> The short Au1–Au2 (2.9653(10) Å) and Au1–Au3 (2.9769(16) Å) distances also indicate noticeable Au–Au contact. The PtAu<sub>3</sub> structure is highly stabilized by six five-membered coordination rings as well as significant Pt–Au and Au–Au interactions.

The different location of Pt(C≡CR)<sub>2</sub> moieties in PtAg<sub>3</sub> and PtAu<sub>3</sub> cluster complexes can be reasonably elucidated on the basis of two factors, including π-acceptor ability of acetylides towards different d<sup>10</sup> metal ions and steric hindrance from tdpmp. It is well-known that silver(I) exhibits more alkynophilicity than gold(I), favoring impressive π-bonding with alkynes.<sup>[31]</sup> The Ag-acetylide linkages through π-bonding facilitate and stabilize PtAg<sub>3</sub> cluster structure (Figure 2a) with the Pt bound to the central P donor in tdpmp so that the Pt is located at the center of the trigonal plane of PtAg<sub>3</sub> cluster. In contrast, the weaker tendency to form Au-acetylide linkages through π-bonding renders that trans-Pt(C≡CR)<sub>2</sub> moiety in PtAu<sub>3</sub> cluster is bound to one of the terminal P donor (Figure 2b) in tdpmp so that the Pt is situated at one apex in the triangle plane of PtAu<sub>3</sub> cluster.

Curiosities to understand the role of chloride in the formation of PtM<sub>3</sub> cluster structures instigated us to perform further studies. The corresponding reactions were thus performed in the presence of Na[BAR<sup>F</sup><sub>4</sub>] (Ar = C<sub>6</sub>H<sub>3</sub>(CF<sub>3</sub>)<sub>2</sub>), which is a typical halide abstracting agent.<sup>[32]</sup> As indicated in Scheme 1, the isolated products became PtM<sub>2</sub> heterotrinnuclear species instead of PtM<sub>3</sub> heterotetranuclear complexes when [BAR<sup>F</sup><sub>4</sub>]<sup>-</sup> was used as counterion in place of ClO<sub>4</sub><sup>-</sup>.

The structures of PtAg<sub>2</sub> complex **11** (Figure 3a) and PtAu<sub>2</sub> complex **12** (Figure 3b) were determined by X-ray crystallography. In the PtAg<sub>2</sub> structure (Figure 3a), the trans-Pt(C≡CC<sub>6</sub>H<sub>4</sub>Bu<sup>t</sup>-4)<sub>2</sub> moiety is bound to the central P donors of two tdpmp ligands to give a square-planar geometry. Each Ag(I) atom is bonded to three terminal P donors of tdpmp and one PPh<sub>3</sub> to show a distorted tetrahedral environment.

Undoubtedly, even if the trans-Pt(C≡CC<sub>6</sub>H<sub>4</sub>Bu<sup>t</sup>-4)<sub>2</sub> moiety in the PtAg<sub>2</sub> complex **11** is bonded to the central P donor of tdpmp as that found in PtAg<sub>3</sub> cluster complexes, the lack of constraint from Ag-Cl-Ag linkage through a bridging chloride could not sufficiently sustain the PtAg<sub>3</sub> cluster structure. Instead, more stable PtAg<sub>2</sub> structure (Figure 3a) forms in the absence of chloride ion. For PtAu<sub>2</sub> complex **12** (Figure 3b), trans-Pt(C≡CC<sub>6</sub>H<sub>3</sub>(CF<sub>3</sub>)<sub>2</sub>-2,4)<sub>2</sub> moiety is bound to the central P atom of tdpmp, in strikingly contrast to that bonded to the terminal P donor found in PtAu<sub>3</sub> cluster structure. It is noteworthy that one of the three terminal P atoms in tdpmp is free of coordination.

Besides the PtM<sub>2</sub> product, another product was also separated through column chromatography, which was identified as [Au(PPh<sub>3</sub>)<sub>2</sub>][BAR<sup>F</sup><sub>4</sub>] when M = Au or [Ag(PPh<sub>3</sub>)<sub>2</sub>][BAR<sup>F</sup><sub>4</sub>] when M = Ag. However, the use of other weaker boron-based anions such as [BPhF<sub>3</sub>]<sup>-</sup> or [BPh<sub>4</sub>]<sup>-</sup> as counterion failed to give PtM<sub>2</sub> heterotrinnuclear products. Instead, only chloride-linked PtM<sub>3</sub> heterotetranuclear cluster complexes were isolated. It should be emphasized that in the presence of Na[BAR<sup>F</sup><sub>4</sub>], only PtM<sub>2</sub> complexes could be isolated, independent of the reactant ratios while PtM<sub>3</sub> cluster complexes could never be obtained. When we attempted to use an excess of Au(tht)Cl or Ag(tht)ClO<sub>4</sub>, we obtained PtM<sub>2</sub> complexes together with [M<sub>4</sub>(tdpmp)<sub>2</sub>]<sup>4+</sup> as the major products reported elsewhere.<sup>[33]</sup> From the investigation mentioned

above, we propose that the participation of Cl<sup>-</sup> in complexation is perturbed by a halide abstracting agent that destabilizes the PtM<sub>3</sub> structure, thus resulting in the formation of PtM<sub>2</sub> species as a stable complex together with a by-product [M(PPh<sub>3</sub>)<sub>x</sub>][BAR<sup>F</sup><sub>4</sub>] (M = Au, x = 2; M = Ag, x = 4). Therefore, we conclude that the participation of chloride in the PtM<sub>3</sub> structure plays a key role in stabilizing the target complexes.

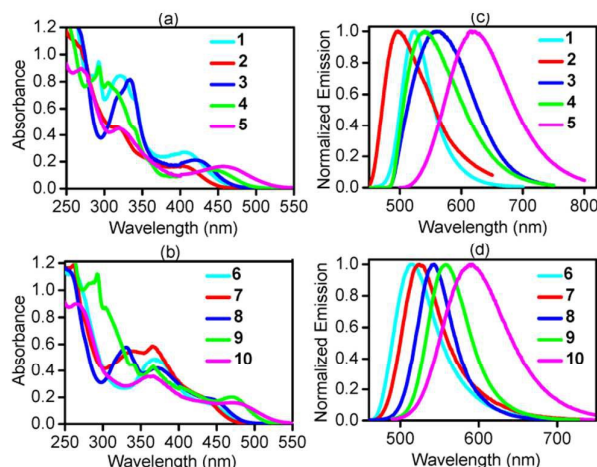


Fig 4 UV-Vis absorption (in fluid CH<sub>2</sub>Cl<sub>2</sub>) and emission spectra (in doped film) of PtM<sub>3</sub> complexes **1–10**.

#### Photophysical Properties

PtM<sub>3</sub> complexes **1–10** (Table 1) in CH<sub>2</sub>Cl<sub>2</sub> exhibit intense UV absorption bands below 290 nm, mainly due to the tdpmp-centered π → π\* transitions. A band centered at 290–360 nm is ascribed to the π → π\* transitions involving carbazole-acetylides. More importantly, a broad low-energy bands above 400 nm (ε ≈ 1.6–1.9 × 10<sup>4</sup> dm<sup>3</sup> mol<sup>-1</sup> cm<sup>-1</sup>) is observed, resulting most likely from aromatic acetylide-to-platinum(II) LMCT (ligand-to-metal charge-transfer) and aromatic acetylide-to-tdpmp LLCT (ligand-to-ligand charge transfer) transitions.<sup>[20,21,23]</sup> The low-energy absorption bands of PtM<sub>3</sub> complexes (Figure 4) were modulated by changing aromatic acetylides. For PtAu<sub>3</sub> complexes (Figure 4b), the low-energy absorption band occurs at 427 nm for **6**, 438 nm for **7**, 443 nm for **8**, 470 nm for **9**, and 472 nm for **10**. Likewise, the absorption bands due to LMCT and LLCT states in PtAg<sub>3</sub> complexes (Figure 4a) appear at 408 nm for **1**, 406 nm for **2**, 426 nm for **3**, 440 nm for **4**, and 458 nm for **5** with almost the same trend as PtAu<sub>3</sub> complexes. The variation trend of low-energy band can be interpreted on the basis of π-conjugation and π-electron donating capability of aromatic acetylides.

PtM<sub>3</sub> complexes **1–10** (Table 1) exhibit unstructured emission bands at around 513–653 nm for PtAg<sub>3</sub> complexes (Figure S1, a) and 524–648 nm for PtAu<sub>3</sub> complexes (Figure S1, b) in fluid CH<sub>2</sub>Cl<sub>2</sub> solutions. The large Stokes shifts with microsecond range of emissive lifetimes indicate a phosphorescent nature with triplet excited states. The emission origin is assigned as the aromatic acetylide-to-

## Journal Name

## ARTICLE

**Table 1.** The UV-Vis absorption and photoluminescent data for PtM<sub>3</sub> cluster complexes 1–10.

complex	$\lambda_{\text{abs}}^{\text{a}}/\text{nm}$ ( $\epsilon/\text{dm}^3 \text{ mol}^{-1} \text{ cm}^{-1}$ )	medium	$\lambda_{\text{em}}/\text{nm}$ ( $\tau/\mu\text{s}$ )	$\Phi_{\text{PL}}/\%$
1	292 (94670), 321 (84310), 340 (66780), 408 (26870)	CH <sub>2</sub> Cl <sub>2</sub>	541 (3.11)	<0.3
		Powder	590 (3.46)	<0.3
		mCP:OXD-7 <sup>b</sup>	522 (4.58)	0.8
2	268 (105300), 318 (46210), 406 (16290)	CH <sub>2</sub> Cl <sub>2</sub>	513 (2.61)	<0.3
		Powder	530 (2.99)	<0.3
		mCP:OXD-7 <sup>b</sup>	472 (2.34)	<0.3
3	262(121360), 334 (81610), 426 (20580)	CH <sub>2</sub> Cl <sub>2</sub>	585 (2.11)	<0.3
		Powder	604 (2.69)	<0.3
		mCP:OXD-7 <sup>b</sup>	560 (4.41)	0.6
4	292 (90800), 304 (77390), 339 (44780), 440 (14040)	CH <sub>2</sub> Cl <sub>2</sub>	562 (2.39)	<0.3
		Powder	590 (2.56)	<0.3
		mCP:OXD-7 <sup>b</sup>	533 (5.43)	2.1
5	268 (89380), 320 (45030), 458 (15870)	CH <sub>2</sub> Cl <sub>2</sub>	653 (1.92)	<0.3
		Powder	687 (2.32)	<0.3
		mCP:OXD-7 <sup>b</sup>	616 (5.39)	3.0
6	292 (88560), 344 (48980), 368 (48180), 427 (16010)	CH <sub>2</sub> Cl <sub>2</sub>	524(2.53)	1.1
		Powder	570 (3.41)	5.1
		mCP:OXD-7 <sup>b</sup>	512(4.90)	90.5
7	263 (111800), 368 (48560), 438 (15590)	CH <sub>2</sub> Cl <sub>2</sub>	528(2.13)	2.6
		Powder	544(2.39)	2.8
		mCP:OXD-7 <sup>b</sup>	522 (3.37)	68.3
8	256(114135), 330 (58018), 373 (41583), 443 (19136)	CH <sub>2</sub> Cl <sub>2</sub>	550 (2.88)	2.6
		Powder	575 (3.60)	7.8
		mCP:OXD-7 <sup>b</sup>	543 (5.11)	88.4
9	281 (104600), 292 (118300), 340 (44660), 366 (43370), 470 (19780)	CH <sub>2</sub> Cl <sub>2</sub>	565(2.37)	9.7
		Powder	592 (3.49)	9.3
		mCP:OXD-7 <sup>b</sup>	559(4.64)	89.3
10	267 (89690), 365 (35630), 472 (16430)	CH <sub>2</sub> Cl <sub>2</sub>	648(1.86)	2.9
		Powder	650 (2.18)	2.4
		mCP:OXD-7 <sup>b</sup>	590 (5.90)	76.8

<sup>a</sup> Absorption spectra were measured in degassed CH<sub>2</sub>Cl<sub>2</sub> solutions with a concentration of  $1 \times 10^{-5}$  M. Absolute quantum yields in powder, films and CH<sub>2</sub>Cl<sub>2</sub> solutions were determined by the integrating sphere (142 mm in diameter). <sup>b</sup> Doped in 48.5 wt% mCP : 48.5 wt% OXD-7 with 3 wt% PtM<sub>3</sub> complex.

platinum(II) <sup>3</sup>LMCT and aromatic acetylide-to-tdpmp <sup>3</sup>LLCT transitions. It is noteworthy that the emission energy of <sup>3</sup>LMCT and <sup>3</sup>LLCT is closely related to the  $\pi$ -electron donating ability of aromatic acetylides. With stronger electron donating phenothiazine attached to acetylide, the emission bands of PtM<sub>3</sub> complexes **5** (653 nm) and **10** (648 nm) show obvious red-shifts compared to those of carbazole-containing complexes (550–585 nm). It is noticeable that PtAu<sub>3</sub>

complexes display much stronger photoluminescence than the corresponding PtAg<sub>3</sub> complexes (Table 1) in both solution and solid state. This is likely due to the lability of Ag–Cl and Ag–C<sub>acetylide</sub> bonds in PtAg<sub>3</sub> cluster complexes, which may serve as a main non-radiative deactivation pathway of the triplet excited state.

The emission spectra of spin-coated films composed of 3 wt% PtAu<sub>3</sub> complex doped in mixed host mCP : OXD-7 (1 : 1)

are centered at 512–590 nm with photoluminescent quantum yields (PLQYs) of 68.3–90.5% (Table 1). Almost identical emission spectra of the doped films to those of the corresponding PtAu<sub>3</sub> complexes in CH<sub>2</sub>Cl<sub>2</sub> solutions with a microsecond region of emissive lifetimes demonstrate a highly efficient energy transfer from organic host materials to PtAu<sub>3</sub> complexes. However, by comparison of the wavelength range and contour of the emission spectra in PtAg<sub>3</sub> complexes (Figure 4c) with those in corresponding PtAu<sub>3</sub> complexes (Figure 4d), the emission energies are comparable but the quantum yields in the formers are quite low (< 3.0%) even after doping with different host materials. The high PLQYs of PtAu<sub>3</sub> complexes ranging from 68.3% to 90.5% in mCP : OXD-7 doped films suggest that they are promising dopants for phosphorescent OLED applications.

The absolute HOMO energy of PtAu<sub>3</sub> complexes **8–10** was determined by electrochemical studies (Figure S2). Anodic sweep shows an irreversible oxidation wave at around +0.80 V with insignificant shifts of the potentials upon modification of aromatic acetylides, assigned as the metal-centered oxidation. Another quasi-reversible oxidation wave at around +1.10 V can be ascribed to the carbazole-based oxidation.<sup>34</sup> The HOMO energy levels of PtAu<sub>3</sub> complexes **8–10** were calculated to be –5.25, –5.26 and –5.23 eV, respectively. The optical band gap of 2.55 eV (**8**), 2.51 eV (**9**) and 2.47 eV (**10**) were extracted from the UV-Vis absorption edge of the corresponding complexes. Adding this band gap to the HOMO energy affords a LUMO level of –2.70, –2.75 and –2.76 eV (Table S9) for PtAu<sub>3</sub> complexes **8–10**, respectively.

### Theoretical Computational Studies

In order to get more insight to the transition characteristics in absorption and emission properties, density functional theory (DFT) and time-dependent DFT (TD-DFT) calculations were carried out using PBE1PBE functional (for computational details, see ESI). The orbital plots depicted in Figure S5 show that the HOMO focuses predominately on aromatic acetylides (>80% population) with some distribution at PtM<sub>3</sub> centers (<12% population) while the LUMO is mostly spread over tdpmp and PtM<sub>3</sub> cluster centers with minor population at aromatic acetylides. The calculations predict that the lowest-energy absorption at 431 nm for **1**, 445 nm for **3**, 405 nm for **6** and 400 nm for **8** (Tables S1, S3, S5 and S7, S1) correlate well with the experimentally measured data. In all the cases, the S<sub>0</sub> → S<sub>1</sub> transition primarily originates from the HOMO → LUMO (HOMO → LUMO+1 for complex **8**), which mainly corresponds to an admixture of LLCT/LMCT character. The calculated excited energies from the ground state to the first triplet excited state are 2.18 eV for **1**, 2.10 eV for **3**, 2.44 eV for **6** and 2.38 eV for **8**, which correspond to the emission wavelengths of 569 nm for **1**, 591 nm for **3**, 509 nm for **6** and 522 nm for **8**. These values coincide well with the experimental data in CH<sub>2</sub>Cl<sub>2</sub> solutions (541 nm for **1**, 585 nm for **3**, 524 nm for **6** and 550 nm for **8**). As indicated in Figure 5, the transition of HOMO → LUMO in lowest-energy triplet states (Tables S2, S4, S6 and S8, S1) is mainly featured with π (aromatic acetylide) → π\*

(tdpmp) <sup>3</sup>LLCT and π (aromatic acetylide) → s/p (PtM<sub>3</sub>) <sup>3</sup>LMCT states, mixed with minor intraligand (<sup>3</sup>IL) character of aromatic acetylide. It is noteworthy that PtAg<sub>3</sub> complexes **1** and **3** display more intraligand (IL) character of aromatic acetylides than PtAu<sub>3</sub> complexes **6** and **8** in both lowest-energy singlet and triplet excited states.

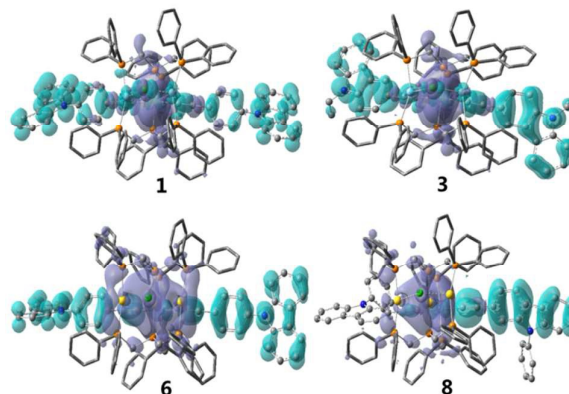


Fig 5 The transition orbital distribution (iso value = 0.0004) in the lowest-energy triplet excited state for PtM<sub>3</sub> complexes **1**, **3**, **6** and **8** in CH<sub>2</sub>Cl<sub>2</sub>. The blue-green and purple regions represent electron depletion (ED) and electron accumulation (EA) in the transition orbitals, respectively.

Table 2. Performance data of solution-processed OLEDs based on PtAu<sub>3</sub> complexes.<sup>a</sup>

compound	<b>8</b>	<b>9</b>	<b>10</b>
$\lambda_{\text{EL}}/\text{nm}$	541	556	588
$V_{\text{on}}^b/\text{V}$	5.2	5.5	4.9
$L_{\text{max}}^c/\text{cd m}^{-2}$	10911	12711	19308
$CE_{\text{max}}^d/\text{cd A}^{-1}$	58.3	62.8	45.2
$PE_{\text{max}}^e/\text{lm W}^{-1}$	26.1	25.1	20.3
$EQE_{\text{max}}^f/\%$	14.9	17.7	18.1
CIE	0.33, 0.61	0.24, 0.51	0.47, 0.52

<sup>a</sup> Device structure is ITO / PEDOT : PSS (50 nm) / mCP (48.5 wt%) : OXD-7 (48.5 wt%) : PtAu<sub>3</sub> complex (3 wt%) (50 nm) / BmPyPb (50 nm) / LiF (1 nm) / Al (100 nm). <sup>b</sup> Turn-on voltage at 1 cd m<sup>-2</sup>. <sup>c</sup> Maximum luminance. <sup>d</sup> Maximum current efficiency. <sup>e</sup> Maximum power efficiency. <sup>f</sup> Maximum external quantum efficiency.

### Solution-Processed OLEDs

Solution-processable OLEDs based on PtAu<sub>3</sub> complexes **8–10** as phosphorescent dopants were investigated using three layer device configuration: ITO / PEDOT : PSS (50 nm) / host : PtAu<sub>3</sub> complex (50 nm) / ETL (50 nm) / LiF (1 nm) / Al (100 nm). The poly(3,4-ethylenedioxythiophene) : poly(styrene-sulfonate) (PEDOT : PSS) was used as a hole-injection layer through spin coating in an aqueous solution. Based on the HOMO (–5.23 to –5.26 eV) and LUMO (–2.70 to –2.76 eV) levels of PtAu<sub>3</sub> complexes **8–10**, mCP (HOMO: –5.90 eV) or TCTA (HOMO: –5.83 eV) and OXD-7 (LUMO: –2.80 eV) were selected to act as blended host materials. To improve the charge balance in the recombination zone, an additional layer with BmPyPb, TPBi or BCP was prepared through thermal deposit to serve as electron transport or hole-blocking layer, then capped with LiF/Al cathode. The HOMO and LUMO levels of the materials used in the devices are schematically depicted in Figure S4. The corresponding electroluminescent (EL) data

are listed in Table 2. The emissive layer was prepared by spin-coating dichloromethane solution of mCP (48.5 wt%) : OXD-7 (48.5 wt%) : PtAu<sub>3</sub> complex (3 wt%).

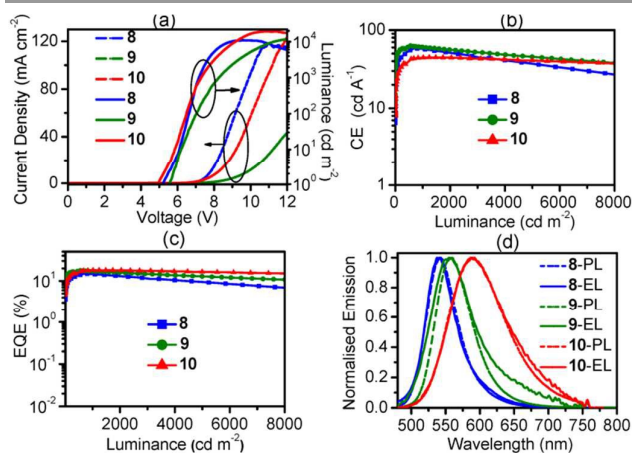


**Fig 6** (a) J–V–L characteristics of the devices based on PtAu<sub>3</sub> complexes 8–10. (b) Current efficiency vs luminance (c) EQE vs luminance. (d) Photoluminescent (PL) spectra (dash) in light-emitting layers and electroluminescent (EL) spectra (solid) of the devices.

The EL spectra show the emission maxima at 541 nm for **8**, 556 nm for **9**, and 588 nm for **10**, coinciding perfectly with the corresponding PL spectra of the emitting films centered at 543 nm for **8**, 559 nm for **9**, and 590 nm for **10**. The excitons are completely confined within the emissive layer and charge carrier recombination takes place only in emissive layers of the devices. The low doping concentration (3 wt%) of PtAu<sub>3</sub> complexes prevents  $\pi$ – $\pi$  interactions between the dopant molecules in devices.<sup>35</sup> As depicted in Figure 6 and Table 2, the optimized devices based on PtAu<sub>3</sub> complex **8** show superior performance with maximum CE of 58.3 cd A<sup>-1</sup> and power efficiency (PE) of 26.1 lm W<sup>-1</sup>, corresponding to peak EQE of 14.9%. The Commission Internationale de L'Éclairage (CIE) chromaticity coordinates (x, y) were evaluated to be (0.33, 0.61), in close proximity to pure green color. Likewise, the optimized devices give a peak CE of 62.8 cd A<sup>-1</sup>, PE of 25.1 lm W<sup>-1</sup> and EQE of 17.7 % for complex **9**, and peak CE of 45.2 cd A<sup>-1</sup>, PE of 20.3 lm W<sup>-1</sup> and EQE of 18.1 % for complex **10**. The performance improvement in CE and EQE for PtAu<sub>3</sub> complex **9** (62.8 cd A<sup>-1</sup> and 17.7%) relative to those for **8** (58.3 cd A<sup>-1</sup> and 14.9%) is presumably derived from the incorporation of one more hole-transport carbazole group, where a better balance in the electron and hole carriers at the emissive interface leads to better device efficiency.

Remarkably, all the devices showed an extremely low efficiency roll-off at practical brightness. The EQE of devices doped with PtAu<sub>3</sub> complex **8** remains as high as 14.4% at luminance of 1000 cd m<sup>-2</sup>, corresponding to EQE roll-off of 3.4%. Likewise, the devices based on PtAu<sub>3</sub> complex **9** also keeps the EQE of 17.1% with a quite low efficiency roll-off of 3.4% at the practical luminance of 1000 cd m<sup>-2</sup>. More importantly, the devices based on PtAu<sub>3</sub> complex **10** displays ultra-low efficiency roll-off. At a luminance of 1000, 2000 and 5000 cd m<sup>-2</sup>, the EQE is 18%, 17.9% and 16.5% with efficiency

roll-off of 0.6%, 1.1% and 8.8%, respectively. The outstanding device performance is owing to better charge carrier balance in the bipolar host interface and negligible exciton annihilation of the dopants with a low doping concentration (3 wt%). It is worth mentioning that the ultra-low EQE roll-off realized in these devices with high EQE (over 18 %) from PtAu<sub>3</sub> complexes is the one among the best solution-processed phosphorescent OLEDs (PHOLEDs).<sup>36</sup>

## Conclusions

A family of tetraphosphine-supported PtM<sub>3</sub> (M = Au, Ag) cluster complexes stabilized by chloride ion abstracted from dichloromethane were prepared and characterized structurally. The bonding difference between gold(I) and silver(I) to acetylide lead to the formation of totally different PtM<sub>3</sub> cluster structures. In contrast to that bound to one of the terminal P donors of P(CH<sub>2</sub>PPh<sub>2</sub>)<sub>3</sub> in PtAu<sub>3</sub> cluster due to steric effect, the Pt(C≡CR)<sub>2</sub> moiety is associated with P(CH<sub>2</sub>PPh<sub>2</sub>)<sub>3</sub> through the central P donor in PtAg<sub>3</sub> cluster complexes, stabilized by the additional Ag–acetylide  $\pi$  bonding interaction. Introducing sodium tetrakis[3,5-bis(trifluoromethyl)phenyl]borate as a halide abstracting agent resulted only in the isolation of PtM<sub>2</sub> complexes. The phosphorescent emission in PtAu<sub>3</sub> complexes is much stronger than that of PtAg<sub>3</sub> complexes because of fluxional structures for the latter. Superior electroluminescence with EQE up to 18.1% is successfully achieved using PtAu<sub>3</sub> cluster complexes as phosphorescent dopants to fabricate solution-processable OLEDs. Most importantly, the optimized devices demonstrate high-efficiency EL performance with extremely small EQE roll-off at practical brightness over 1000 cd m<sup>-2</sup>.

## Experimental Section

### General Procedures and Materials

All reactions were operated under dry argon using Schlenk techniques and vacuum-line systems. Solvents were carefully dried and distilled from appropriate drying agents prior to use. Commercially available reagents were used without further purification unless stated otherwise. Sonogashira coupling reactions were utilized to prepare the alkynyl ligands such as 9-(4-ethynylphenyl)-9H-carbazole (HC≡C-4-C<sub>6</sub>H<sub>4</sub>Carb-9), 9-phenyl-2-ethynyl-9H-carbazole (HC≡C-2-PhCarb-9), 9-(4-(9H-carbazol-9-yl)phenyl)-3-ethynyl-9H-carbazole (HC≡C-3-CarbPhCarb-9), 10-ethyl-3-ethynyl-10H-phenothiazine (HC≡C-3-EtPTZ-9). The precursor complexes Pt(PPh<sub>3</sub>)<sub>2</sub>(C≡C-4-C<sub>6</sub>H<sub>4</sub>Carb-9)<sub>2</sub>, Pt(PPh<sub>3</sub>)<sub>2</sub>(C≡CC<sub>6</sub>H<sub>4</sub>Bu<sup>t</sup>-4)<sub>2</sub>, Pt(PPh<sub>3</sub>)<sub>2</sub>(C≡C-2-PhCarb-9)<sub>2</sub>, Pt(PPh<sub>3</sub>)<sub>2</sub>(C≡C-3-CarbPhCarb-9)<sub>2</sub>, and Pt(PPh<sub>3</sub>)<sub>2</sub>(C≡C-3-EtPTZ-9)<sub>2</sub> were prepared by reactions of Pt(PPh<sub>3</sub>)<sub>2</sub>Cl<sub>2</sub> (0.5 mmol), corresponding alkynyl ligands (1.1 mmol), CuI (1 mg) and NEt<sub>3</sub> (1 mL) in chloroform (50 mL) with stirring at 50 °C for 5 h. The procedure for the synthesis of tris((diphenylphosphino)methyl)phosphine (tdmp) followed the methods reported in the literatures.<sup>38,39</sup> All reactions were monitored by using thin-layer chromatography (TLC) with Merck precoated glass plates. The products were visualized with UV-light irradiation at 254 and 365 nm.

[PtAg<sub>3</sub>( $\mu$ -Cl)(tdmp)<sub>2</sub>(C≡C-4-C<sub>6</sub>H<sub>4</sub>Carb-9)<sub>2</sub>](ClO<sub>4</sub>)<sub>2</sub> (**1**). A mixture of Pt(PPh<sub>3</sub>)<sub>2</sub>(C≡C-4-C<sub>6</sub>H<sub>4</sub>Carb-9)<sub>2</sub> (62.6 mg, 0.05 mmol), tdmp (62.8 mg, 0.1 mmol), and Ag(tht)ClO<sub>4</sub> (45 mg, 0.15 mmol) was added to CH<sub>2</sub>Cl<sub>2</sub> (30 mL) and the solution was stirred at ambient temperature for 8 h. The product was then purified by chromatography on a silica gel column using CH<sub>2</sub>Cl<sub>2</sub>-MeOH

(*v/v* = 20 : 1) as the eluent to give pure sample. Yield: 76%. <sup>1</sup>H NMR (CDCl<sub>3</sub>, ppm): 8.20 (d, 4H, *J* = 7.8 Hz), 7.87–7.91 (m, 8H), 7.69–7.72 (m, 14H), 7.48–7.51 (m, 10H), 7.35–7.38 (m, 10H), 7.29–7.33 (m, 18H), 7.20–7.23 (m, 12H), 6.66 (t, 4H, *J* = 6.4 Hz), 5.19 (d, 4H, *J* = 8.4 Hz), 4.17 (br, 4H), 3.46 (br, 8H). <sup>31</sup>P[<sup>1</sup>H] NMR (CDCl<sub>3</sub>, ppm): 19.3 (m, 2P, *J*<sub>P-P</sub> = 27 Hz, *J*<sub>Pt-P</sub> = 2402 Hz), 9.6 (m, 2P, *J*<sub>P-P</sub> = 37 Hz), –0.6 (m, 4P). HRMS (ESI): *m/z* calculated for C<sub>118</sub>H<sub>96</sub>Ag<sub>3</sub>ClN<sub>2</sub>P<sub>8</sub>Pt [M–2ClO<sub>4</sub>]<sup>2+</sup>: 1172.0958; found: 1172.0993. IR (KBr, cm<sup>-1</sup>): 2084w (C≡C), 1098s (ClO<sub>4</sub><sup>-</sup>).

**[PtAg<sub>3</sub>(μ-Cl)(tdpmp)<sub>2</sub>(C≡CC<sub>6</sub>H<sub>4</sub>Bu<sup>1-4</sup>)<sub>2</sub>](ClO<sub>4</sub>)<sub>2</sub> (2).** This compound was prepared by the same synthetic procedure as that of **1** except for the use of Pt(PPh<sub>3</sub>)<sub>2</sub>(C≡CC<sub>6</sub>H<sub>4</sub>Bu<sup>1-4</sup>)<sub>2</sub> instead of Pt(PPh<sub>3</sub>)<sub>2</sub>(C≡C–4–C<sub>6</sub>H<sub>4</sub>Carb–9)<sub>2</sub>. Yield: 84%. <sup>1</sup>H NMR (CDCl<sub>3</sub>, ppm): 7.74–7.78 (m, 14H), 7.53–7.56 (m, 10H), 7.43–7.46 (m, 4H), 7.29–7.33 (m, 14H), 7.18–7.21 (m, 10H), 7.09–7.12 (m, 8H), 6.20 (d, 4H, *J* = 8 Hz), 4.91 (d, 4H, *J* = 8 Hz), 3.96 (br, 4H), 3.31 (br, 4H), 3.10 (br, 4H), 0.96–1.2 (m, 18H). <sup>31</sup>P[<sup>1</sup>H] NMR (CDCl<sub>3</sub>, ppm): 19.1 (m, 2P, *J*<sub>P-P</sub> = 27 Hz, *J*<sub>Pt-P</sub> = 2344 Hz), 9.0 (m, 2P, *J*<sub>P-P</sub> = 38 Hz), –4.0 (m, 4P). HRMS (ESI): *m/z* calculated for C<sub>102</sub>H<sub>98</sub>Ag<sub>3</sub>ClP<sub>8</sub>Pt [M–2ClO<sub>4</sub>]<sup>2+</sup>: 1063.1005; found: 1063.1009. IR (KBr, cm<sup>-1</sup>): 2082w (C≡C), 1098s (ClO<sub>4</sub><sup>-</sup>).

**[PtAg<sub>3</sub>(μ-Cl)(tdpmp)<sub>2</sub>(C≡C–3–EtCarb–9)<sub>2</sub>](ClO<sub>4</sub>)<sub>2</sub> (3).** This compound was prepared by the same synthetic procedure as that of **1** except for the use of trans-Pt(PPh<sub>3</sub>)<sub>2</sub>(C≡C–3–EtCarb–9)<sub>2</sub> instead of Pt(PPh<sub>3</sub>)<sub>2</sub>(C≡C–4–C<sub>6</sub>H<sub>4</sub>Carb–9)<sub>2</sub>. Yield: 75%. <sup>1</sup>H NMR (CDCl<sub>3</sub>, ppm): 7.81–7.84 (m, 8H), 7.72–7.75 (m, 6H), 7.64–7.67 (m, 8H), 7.37–7.40 (m, 6H), 7.32–7.36 (m, 12H), 7.24–7.27 (m, 6H), 7.19–7.22 (m, 12H), 7.07–7.10 (m, 10H), 6.32 (d, 2H, *J* = 8.6 Hz), 5.96 (s, 2H), 5.11 (d, 2H, *J* = 8.2 Hz), 4.29 (q, 4H, *J* = 7.2 Hz), 4.25 (br, 4H), 3.45 (br, 4H), 3.29 (br, 4H), 1.43 (t, 6H, *J* = 7.2 Hz). <sup>31</sup>P[<sup>1</sup>H] NMR (CDCl<sub>3</sub>, ppm): 18.9 (m, 2P, *J*<sub>P-P</sub> = 28 Hz, *J*<sub>Pt-P</sub> = 2406 Hz), 9.3 (m, 2P, *J*<sub>P-P</sub> = 37 Hz), –1.8 (m, 4P, *J*<sub>P-P</sub> = 31 Hz). HRMS (ESI): *m/z* calculated for C<sub>110</sub>H<sub>96</sub>Ag<sub>3</sub>ClN<sub>2</sub>P<sub>8</sub>Pt [M–2ClO<sub>4</sub>]<sup>2+</sup>: 1124.0958; found: 1124.0975. IR (KBr, cm<sup>-1</sup>): 2071w (C≡C), 1098s (ClO<sub>4</sub><sup>-</sup>).

**[PtAg<sub>3</sub>(μ-Cl)(tdpmp)<sub>2</sub>(C≡C–3–CarbPhCarb–9)<sub>2</sub>](ClO<sub>4</sub>)<sub>2</sub> (4).** This compound was prepared by the same synthetic procedure as that of **1** except for the use of Pt(PPh<sub>3</sub>)<sub>2</sub>(C≡C–3–CarbPhCarb–9)<sub>2</sub> instead of Pt(PPh<sub>3</sub>)<sub>2</sub>(C≡C–4–C<sub>6</sub>H<sub>4</sub>Carb–9)<sub>2</sub>. Yield: 72%. <sup>1</sup>H NMR (CDCl<sub>3</sub>, ppm): 8.24 (d, 2H, *J* = 7.8 Hz), 7.91–7.94 (m, 12H), 7.73–7.78 (m, 18H), 7.62–7.65 (m, 4H), 7.51–7.54 (m, 8H), 7.40–7.44 (m, 8H), 7.31–7.35 (m, 16H), 7.24–7.27 (m, 14H), 7.13–7.16 (m, 10H), 6.47 (d, 2H, *J* = 8.6 Hz), 6.05 (s, 2H), 5.15 (d, 2H, *J* = 7.8 Hz), 4.28 (br, 4H), 3.48 (br, 4H), 3.33 (br, 4H). <sup>31</sup>P[<sup>1</sup>H] NMR (CDCl<sub>3</sub>, ppm): 18.9 (m, 2P, *J*<sub>P-P</sub> = 27 Hz, *J*<sub>Pt-P</sub> = 2302 Hz), 9.3 (m, 2P, *J*<sub>P-P</sub> = 37.6 Hz), –3.4 (m, 4P, *J*<sub>P-P</sub> = 28 Hz). HRMS (ESI): *m/z* calculated for C<sub>142</sub>H<sub>110</sub>Ag<sub>3</sub>ClN<sub>4</sub>P<sub>8</sub>Pt [M–2ClO<sub>4</sub>]<sup>2+</sup>: 1337.1536; found: 1337.1550. IR (KBr, cm<sup>-1</sup>): 2071w (C≡C), 1098s (ClO<sub>4</sub><sup>-</sup>).

**[PtAg<sub>3</sub>(μ-Cl)(tdpmp)<sub>2</sub>(C≡C–3–EtPTZ–9)<sub>2</sub>](ClO<sub>4</sub>)<sub>2</sub> (5).** This compound was prepared by the same synthetic procedure as that of **1** except for the use of Pt(PPh<sub>3</sub>)<sub>2</sub>(C≡C–3–EtPTZ–9)<sub>2</sub> instead of Pt(PPh<sub>3</sub>)<sub>2</sub>(C≡C–4–C<sub>6</sub>H<sub>4</sub>Carb–9)<sub>2</sub>. Yield: 78%. <sup>1</sup>H NMR (CDCl<sub>3</sub>, ppm): 8.05 (d, 2H, *J* = 7.8 Hz), 7.91–7.94 (m, 8H), 7.72–7.76 (m, 6H), 7.54–7.57 (m, 8H), 7.38–7.42 (m, 10H), 7.23–7.28 (m, 20H), 7.13–7.16 (m, 6H), 7.01–7.04 (m, 10H), 5.58 (s, 2H), 5.05 (d, 2H, *J* = 8.2 Hz), 4.23 (br, 4H), 3.39 (q, 4H, *J* = 7.2 Hz), 3.23 (br, 8H), 1.05 (t, 6H, *J* = 7.2 Hz). <sup>31</sup>P[<sup>1</sup>H] NMR (CDCl<sub>3</sub>, ppm): 18.0 (m, 2P, *J*<sub>P-P</sub> = 27 Hz, *J*<sub>Pt-P</sub> = 2336 Hz), 9.1 (m, 2P, *J*<sub>P-P</sub> = 31 Hz), –2.2 (m, 4P). HRMS (ESI): *m/z* calculated for C<sub>110</sub>H<sub>96</sub>Ag<sub>3</sub>ClN<sub>2</sub>P<sub>8</sub>PS<sub>2</sub> [M–2ClO<sub>4</sub>]<sup>2+</sup>: 1156.0678; found: 1156.0700. IR (KBr, cm<sup>-1</sup>): 2092w (C≡C), 1096s (ClO<sub>4</sub><sup>-</sup>).

**[PtAu<sub>3</sub>(μ-Cl)(tdpmp)<sub>2</sub>(C≡C–4–C<sub>6</sub>H<sub>4</sub>Carb–9)<sub>2</sub>](ClO<sub>4</sub>)<sub>2</sub> (6).** A mixture of Pt(PPh<sub>3</sub>)<sub>2</sub>(C≡C–4–C<sub>6</sub>H<sub>4</sub>Carb–9)<sub>2</sub> (62.6 mg, 0.05 mmol), tdpmp (62.8 mg, 0.1 mmol), Au(tht)Cl (48 mg, 0.15 mmol), NH<sub>4</sub>ClO<sub>4</sub> (18 mg, 0.15 mmol) was added to CH<sub>2</sub>Cl<sub>2</sub> (30 mL) and the solution was stirred at ambient temperature for 8 h. The product was then purified by chromatography on a silica gel column using CH<sub>2</sub>Cl<sub>2</sub>–MeOH (*v/v* = 20 : 1) as the eluent to give pure solid. Yield: 68%. <sup>1</sup>H NMR (CDCl<sub>3</sub>, ppm): 8.18 (d, 4H, *J* = 7.8 Hz), 7.93–7.97 (m, 16H), 7.72 (d, 8H, *J* = 6.8 Hz), 7.50–7.54 (m, 16H), 7.39–7.42 (m, 14H), 7.31–7.34 (m, 10H), 7.16 (t, 8H, *J* = 7.6 Hz), 6.90 (d, 4H, *J* = 8.4 Hz), 5.70

(d, 4H, *J* = 8.4 Hz), 4.17 (br, 4H), 3.67 (br, 8H). <sup>31</sup>P[<sup>1</sup>H] NMR (CDCl<sub>3</sub>, ppm): 30.4 (t, 4P, *J*<sub>P-P</sub> = 31 Hz), 22.7 (m, 2P, *J*<sub>P-P</sub> = 25 Hz), 4.2 (t, 2P, *J*<sub>P-P</sub> = 25 Hz, *J*<sub>Pt-P</sub> = 2676 Hz). HRMS (ESI): *m/z* calculated for C<sub>118</sub>H<sub>96</sub>Au<sub>3</sub>ClN<sub>2</sub>P<sub>8</sub>Pt [M–2ClO<sub>4</sub>]<sup>2+</sup>: 1305.1880; found: 1305.1839. IR (KBr, cm<sup>-1</sup>): 2107w (C≡C), 1100s (ClO<sub>4</sub><sup>-</sup>).

**[PtAu<sub>3</sub>(μ-Cl)(tdpmp)<sub>2</sub>(C≡CC<sub>6</sub>H<sub>4</sub>Bu<sup>1-4</sup>)<sub>2</sub>](ClO<sub>4</sub>)<sub>2</sub> (7).** This compound was prepared by the same synthetic procedure as that of **6** except for the use of Pt(PPh<sub>3</sub>)<sub>2</sub>(C≡CC<sub>6</sub>H<sub>4</sub>Bu<sup>1-4</sup>)<sub>2</sub> instead of Pt(PPh<sub>3</sub>)<sub>2</sub>(C≡C–4–C<sub>6</sub>H<sub>4</sub>Carb–9)<sub>2</sub>. Yield: 72%. <sup>1</sup>H NMR (CDCl<sub>3</sub>, ppm): 7.89–7.93 (m, 8H), 7.74–7.77 (m, 8H), 7.66–7.70 (m, 8H), 7.49–7.52 (m, 14H), 7.31–7.34 (m, 14H), 7.02–7.05 (m, 8H), 6.54 (d, 4H, *J* = 8 Hz), 5.41 (d, 4H, *J* = 8 Hz), 4.08 (br, 4H), 3.85 (br, 4H), 3.54 (br, 4H), 0.98–1.2 (m, 18H). <sup>31</sup>P[<sup>1</sup>H] NMR (CDCl<sub>3</sub>, ppm): 29.1 (t, 4P, *J*<sub>P-P</sub> = 32 Hz), 17.8 (m, 2P, *J*<sub>P-P</sub> = 30 Hz), 4.8 (t, 2P, *J*<sub>P-P</sub> = 27 Hz, *J*<sub>Pt-P</sub> = 2694 Hz). HRMS (ESI): *m/z* calculated for C<sub>102</sub>H<sub>98</sub>Au<sub>3</sub>ClN<sub>2</sub>P<sub>8</sub>Pt [M–2ClO<sub>4</sub>]<sup>2+</sup>: 1196.1927; found: 1196.1925. IR (KBr, cm<sup>-1</sup>): 2105w (C≡C), 1100s (ClO<sub>4</sub><sup>-</sup>).

**[PtAu<sub>3</sub>(μ-Cl)(tdpmp)<sub>2</sub>(C≡C–2–PhCarb–9)<sub>2</sub>](ClO<sub>4</sub>)<sub>2</sub> (8).** This compound was prepared by the same synthetic procedure as that of **6** except for the use of trans-Pt(PPh<sub>3</sub>)<sub>2</sub>(C≡C–2–PhCarb–9)<sub>2</sub> instead of Pt(PPh<sub>3</sub>)<sub>2</sub>(C≡C–4–C<sub>6</sub>H<sub>4</sub>Carb–9)<sub>2</sub>. Yield: 66%. <sup>1</sup>H NMR (CDCl<sub>3</sub>, ppm): 8.01–8.03 (m, 8H), 7.74–7.77 (m, 10H), 7.66–7.69 (m, 10H), 7.51–7.55 (m, 12H), 7.43–7.49 (m, 12H), 7.37–7.41 (m, 16H), 6.95 (m, 10H), 6.78 (d, 2H, *J* = 8.4 Hz), 6.02 (s, 2H), 5.78 (d, 2H, *J* = 8.4 Hz), 4.13 (br, 4H), 4.03 (br, 4H), 3.65 (br, 4H). <sup>31</sup>P[<sup>1</sup>H] NMR (CDCl<sub>3</sub>, ppm): 29.6 (t, 4P, *J*<sub>P-P</sub> = 32 Hz), 18.1 (m, 2P, *J*<sub>P-P</sub> = 30 Hz), 6.2 (t, 2P, *J*<sub>P-P</sub> = 30 Hz, *J*<sub>Pt-P</sub> = 2726 Hz). HRMS (ESI): *m/z* calculated for C<sub>118</sub>H<sub>96</sub>Au<sub>3</sub>ClN<sub>2</sub>P<sub>8</sub>Pt [M–2ClO<sub>4</sub>]<sup>2+</sup>: 1305.1880; found: 1305.1909. IR (KBr, cm<sup>-1</sup>): 2099w (C≡C), 1100s (ClO<sub>4</sub><sup>-</sup>).

**[PtAu<sub>3</sub>(μ-Cl)(tdpmp)<sub>2</sub>(C≡C–3–CarbPhCarb–9)<sub>2</sub>](ClO<sub>4</sub>)<sub>2</sub> (9).** This compound was prepared by the same synthetic procedure as that of **6** except for the use of trans-Pt(PPh<sub>3</sub>)<sub>2</sub>(C≡C–3–CarbPhCarb–9)<sub>2</sub> instead of Pt(PPh<sub>3</sub>)<sub>2</sub>(C≡C–4–C<sub>6</sub>H<sub>4</sub>Carb–9)<sub>2</sub>. Yield: 65%. <sup>1</sup>H NMR (CDCl<sub>3</sub>, ppm): 8.23 (d, 4H, *J* = 7.6 Hz), 8.04–8.07 (m, 8H), 7.87–7.90 (m, 6H), 7.76–7.81 (m, 18H), 7.58–7.61 (m, 10H), 7.48–7.52 (m, 14H), 7.42–7.47 (m, 20H), 7.02–7.05 (m, 10H), 6.95 (d, 4H, *J* = 8.6 Hz), 6.05 (s, 2H), 5.91 (d, 2H, *J* = 8.6 Hz), 4.16 (br, 4H), 4.06 (br, 4H), 3.68 (br, 4H). <sup>31</sup>P[<sup>1</sup>H] NMR (CDCl<sub>3</sub>, ppm): 29.7 (t, 4P, *J*<sub>P-P</sub> = 32 Hz), 18.2 (m, 2P, *J*<sub>P-P</sub> = 30 Hz), 6.2 (t, 2P, *J*<sub>P-P</sub> = 27 Hz, *J*<sub>Pt-P</sub> = 2706 Hz). HRMS (ESI): *m/z* calculated for C<sub>142</sub>H<sub>110</sub>Au<sub>3</sub>ClN<sub>4</sub>P<sub>8</sub>Pt [M–2ClO<sub>4</sub>]<sup>2+</sup>: 1470.7458; found: 1470.7484. IR (KBr, cm<sup>-1</sup>): 2104w (C≡C), 1100s (ClO<sub>4</sub><sup>-</sup>).

**[PtAu<sub>3</sub>(μ-Cl)(tdpmp)<sub>2</sub>(C≡C–3–EtPTZ–9)<sub>2</sub>](ClO<sub>4</sub>)<sub>2</sub> (10).** This compound was prepared by the same synthetic procedure as that of **6** except for the use of Pt(PPh<sub>3</sub>)<sub>2</sub>(C≡C–3–EtPTZ–9)<sub>2</sub> instead of Pt(PPh<sub>3</sub>)<sub>2</sub>(C≡C–4–C<sub>6</sub>H<sub>4</sub>Carb–9)<sub>2</sub>. Yield: 70%. <sup>1</sup>H NMR (CDCl<sub>3</sub>, ppm): 7.87–7.89 (m, 8H), 7.74–7.77 (m, 8H), 7.66–7.69 (m, 8H), 7.48–7.51 (m, 12H), 7.36–7.39 (m, 12H), 7.12–7.15 (m, 16H), 6.95 (t, 2H, *J* = 7.2 Hz), 6.86 (d, 2H, *J* = 8.2 Hz), 6.18 (d, 2H, *J* = 8.4 Hz), 5.35 (d, 2H, *J* = 8.4 Hz), 5.04 (s, 2H), 4.04 (br, 4H), 3.93 (br, 4H), 3.84 (q, 4H, *J* = 7.0 Hz), 3.54 (br, 4H), 1.41 (t, 6H, *J* = 7.0 Hz). <sup>31</sup>P[<sup>1</sup>H] NMR (CDCl<sub>3</sub>, ppm): 29.6 (t, 4P, *J*<sub>P-P</sub> = 32 Hz), 18.4 (m, 2P, *J*<sub>P-P</sub> = 30 Hz), 5.8 (t, 2P, *J*<sub>P-P</sub> = 29 Hz, *J*<sub>Pt-P</sub> = 2706 Hz). HRMS (ESI): *m/z* calculated for C<sub>110</sub>H<sub>96</sub>Au<sub>3</sub>ClN<sub>2</sub>P<sub>8</sub>PS<sub>2</sub> [M–2ClO<sub>4</sub>]<sup>2+</sup>: 1289.1600; found: 1289.1617. IR (KBr, cm<sup>-1</sup>): 2099w (C≡C), 1100s (ClO<sub>4</sub><sup>-</sup>).

**[PtAg<sub>2</sub>(tdpmp)<sub>2</sub>(PPh<sub>3</sub>)<sub>2</sub>(C≡CC<sub>6</sub>H<sub>4</sub>Bu<sup>1-4</sup>)<sub>2</sub>](BAR<sup>F</sup><sub>4</sub>)<sub>2</sub> (11).** A mixture of Pt(PPh<sub>3</sub>)<sub>2</sub>(C≡CC<sub>6</sub>H<sub>4</sub>Bu<sup>1-4</sup>)<sub>2</sub> (51.7 mg, 0.05 mmol), tdpmp (62.8 mg, 0.1 mmol), Ag(tht)ClO<sub>4</sub> (45 mg, 0.15 mmol) and NaBAR<sup>F</sup><sub>4</sub> (133 mg, 0.15 mmol) was added to CH<sub>2</sub>Cl<sub>2</sub> (30 mL) and the solution was stirred at ambient temperature for 8 h. The product was then purified by chromatography on a silica gel column using Petroleum ether : CH<sub>2</sub>Cl<sub>2</sub> (*v/v* = 1 : 1) as the eluent to give pure sample. yield 74%; <sup>1</sup>H NMR (CD<sub>3</sub>CN, ppm): 7.74 (m, 18H), 7.52 (m, 24H), 7.47 (d, 4H, *J* = 8.4 Hz), 7.31 (m, 4H), 7.28 (m, 22H), 7.18 (d, 4H, *J* = 8.4 Hz), 6.97 (m, 22H), 6.91 (m, 24H), 3.60 (br, 12H), 1.32 (s, 18H). <sup>31</sup>P NMR (CD<sub>3</sub>CN, ppm): 16.9 (m, 1P), 14.5 (m, 1P), –2.8 (s, 2P, *J*<sub>Pt-P</sub> = 2434 Hz), –14.9 (m, 3P), –16.1 (m, 3P). <sup>19</sup>F NMR (CD<sub>3</sub>CN, ppm): –62.3 (s). HRMS

(ESI):  $m/z$  calculated for  $C_{138}H_{128}Ag_2Pt_{10}$  [M - 2BAR<sup>F</sup><sub>4</sub>]<sup>2+</sup>: 1253.2547; found: 1253.2581.

[PtAu<sub>2</sub>(tdpmp)<sub>2</sub>(C≡C- Ph(2,4-CF<sub>3</sub>)<sub>2</sub>)(Cl)(BAR<sup>F</sup><sub>4</sub>) (12). A mixture of Pt(PPh<sub>3</sub>)<sub>2</sub>(C≡CPh(2,4-CF<sub>3</sub>)<sub>2</sub>) (59.6 mg, 0.05 mmol), tdpmp (62.8 mg, 0.1 mmol), Au(tht)Cl (48 mg, 0.15 mmol), NaBAR<sup>F</sup><sub>4</sub> (133 mg, 0.15 mmol) was added to CH<sub>2</sub>Cl<sub>2</sub> (30 mL) and the solution was stirred at ambient temperature for 8 h. The product was then purified by chromatography on a silica gel column using Petroleum ether : CH<sub>2</sub>Cl<sub>2</sub> (v/v = 1 : 1) as the eluent to give pure solid, yield 62%; <sup>1</sup>H NMR (CD<sub>3</sub>CN, ppm): 7.77 (s, 2H), 7.71 (br, 16H), 7.69 (s, 8H), 7.51 (br, 20H), 7.41 (s, 2H), 7.38 (d, 10H, J = 7.6 Hz), 7.30 (t, 18H, J = 7.6 Hz), 6.20 (d, 2H, J = 8.4 Hz), 3.66 (br, 12H). <sup>31</sup>P NMR (CD<sub>3</sub>CN, ppm): 11.6 (br, 6P), 3.6 (m, 2P, J<sub>Pt-P</sub> = 2426 Hz). <sup>19</sup>F NMR (CD<sub>3</sub>CN, ppm): -61.8 (s), -63.2 (s), -63.4 (s). HRMS (ESI):  $m/z$  calculated for C<sub>98</sub>H<sub>78</sub>Au<sub>2</sub>F<sub>12</sub>P<sub>8</sub>Pt [M - (Cl)(BAR<sup>F</sup><sub>4</sub>)]<sup>2+</sup>: 1160.1372; found: 1160.1405.

**Physical Measurements.** <sup>1</sup>H and <sup>31</sup>P NMR spectra were performed on a Bruker Avance III (400 MHz) spectrometer with SiMe<sub>4</sub> as the internal reference and H<sub>3</sub>PO<sub>4</sub> as the external reference, respectively. Chemical shifts are reported in parts per million (ppm) downfield from residual solvent peaks and coupling constants are reported as Hertz (Hz). Splitting patterns are designated as singlet (s), doublet (d) and triplet (t). Splitting patterns that could not be interpreted or easily visualized are designated as multiplet (m) and broad (br). UV-Vis absorption spectra were measured on a Perkin-Elmer Lambda 35 UV-Vis spectrophotometer using a 10 mm path quartz cell. Infrared spectra (IR) were recorded on a Magna 750 FT-IR spectrophotometer. High-resolution mass spectrometry (HRMS) was recorded on an Impact II mass spectrometer using dichloromethane and methanol mixtures as mobile phases. The excitation and emission spectra together with the emissive lifetimes were measured on Edinburgh FLS-920 fluorescence spectrometer. Emission spectra were recorded by exciting the samples at their absorption maximum unless otherwise mentioned. All the experiments in solutions were performed at a concentration of 1 × 10<sup>-5</sup> M. The luminescent quantum yield (Φ<sub>PL</sub>) in degassed dichloromethane solutions, powder samples and films at room temperature were determined by the integrating sphere (142 mm in diameter) using Edinburgh FLS-920 fluorescence spectrometer. Cyclic voltammetry was measured on CHI 660E electrochemical workstation (Shanghai CH Instruments) in CH<sub>2</sub>Cl<sub>2</sub> solution using 0.1 M tetrabutylammonium hexafluorophosphate (TBAPF<sub>6</sub>) as the supporting electrolyte. The experiments were performed at room temperature at 1 mM concentration with a three-electrode cell that consisted of a Pt wire as an auxiliary electrode, a saturated Ag/Ag<sup>+</sup> reference electrode and a glassy graphite working electrode. Ferrocene/ferrocenium (Fc/Fc<sup>+</sup>) was used as an internal standard. Thermogravimetric analysis (TGA) was performed under a continuous nitrogen flow using a TA Instruments Q50 at a heating rate of 10 °C min<sup>-1</sup>.

**Crystal Structural Determination.** X-ray single-crystal diffraction data were collected on a Bruker D8 Venture diffractometer using IμS 3.0 microfocus source Mo-Kα radiation (λ = 0.71073 Å) and PHOTON II CPAD detector. Frames were integrated with the Bruker SAINT software package (V8.38A) using a SAINT algorithm. Data were corrected for absorption effects using the multi-scan method (SADABS).<sup>3</sup> The structure was solved and refined using the Bruker SHELXTL Software Package, a computer program for automatic solution of crystal structures, and refined by the full-matrix least-squares method with ShelXle Version 4.8.6, a Qt graphical user interface for the SHELXL.<sup>39</sup>

**Computational Details.** To understand the electronic and spectroscopic properties, the calculations were implemented by using Gaussian 09 program package<sup>40</sup> for compounds **1**, **3**, **6** and **8**. The geometrical structures as isolated molecules in the ground state and the lowest-energy triplet state were firstly optimized, respectively, by the restricted and unrestricted density functional theory (DFT) method with the gradient corrected correlation functional PBE1PBE.<sup>41</sup> During the optimization process, the convergent values of maximum force, root-mean-square (RMS) force, maximum displacement and RMS displacement were set by default. To analyze the spectroscopic

properties, 80 singlet and 6 triplet excited-states were calculated, respectively, based on the optimized structures in the ground state and lowest-energy triplet state to determine the vertical excitation energies by time-dependent density functional theory (TD-DFT)<sup>42</sup> with the same functional used in the optimization process. In the calculation of excited states, the polarizable continuum model method (PCM)<sup>43</sup> using CH<sub>2</sub>Cl<sub>2</sub> as the solvent was employed. The self-consistent field (SCF) convergence criterions of RMS density matrix and maximum density matrix were set at 10<sup>-8</sup> and 10<sup>-6</sup> a.u., respectively, in excited-state calculation. The iterations of excited states continue until the changes on energies of states were no more than 10<sup>-7</sup> a.u. between the iterations, and then convergences were reached in all the excited states. In these calculations, the Stuttgart-Dresden (SDD)<sup>44</sup> basis set and the effective core potentials (ECPs) were used to describe the Pt, Ag and Au atoms. Other non-metal atoms of Cl, P, N, C and H were described by the all-electron basis set of 6-31G\*. Visualization of the frontier molecular orbitals and the transition orbital distribution were performed by GaussView. Ros & Schuit method<sup>45</sup> (C-squared population analysis method, SCPA) was supported to analyze the partition orbital composition by using Multiwfn 3.3.8 program.<sup>46</sup>

**Device Fabrication and characterization:** ITO substrates were cleaned by detergent and deionized water, then successively washed by ethanol, acetone and isopropanol under ultrasonic, respectively, followed by UV-ozone treatment for 15 min. A PEDOT : PSS solution was spin-coated on the ITO substrates at 4800 r/min for 1 min, which were then dried at 140 °C for 20 min. The emitting layers were prepared using filtered CH<sub>2</sub>Cl<sub>2</sub> solutions (5 mg/mL) composed of host and PtAu<sub>3</sub> compound through spin-coating at 2000 r/min for 30 s. Subsequently, ETL (0.3 nm/s), LiF (0.05 nm/s) and Al (3 nm/s) were thermally evaporated in a vacuum chamber at a base pressure lower than 4.0 × 10<sup>-4</sup> Pa. The current density-voltage-brightness (I-V-B) characteristics of the devices were measured on a Keithley 2400/2000 source meter with a calibrated silicon photodiode. All the measurements of the devices were performed at dry and ambient conditions with humidity lower than 30%.

## Acknowledgements

We are grateful for financial support from the National Natural Science Foundation of China (Grants 21650110449, U1405252, 21531008, 21601184 and 21473201), the 973 Project from MSTC (Grant 2014CB845603), the CAS/SAFEA International Partnership Program for Creative Research Teams, and the Strategic Priority Research Program of the Chinese Academy of Sciences (Grant XDB20000000).

## Notes and references

- (a) C. Adachi, M. A. Baldo, M. E. Thompson, S. R. Forrest, J. Appl. Phys., 2001, **90**, 5048; (b) S.-L. Lai, W.-Y. Tong, S. C. F. Kui, M.-Y. Chan, C.-C. Kwok, C.-M. Che, Adv. Funct. Mater., 2013, **23**, 5168; (c) Y. Chi, P.-T. Chou, Chem. Soc. Rev., 2010, **39**, 638; (d) K.-H. Kim, J.-L. Liao, S. W. Lee, B. Sim, C.-K. Moon, G.-H. Lee, H. J. Kim, Y. Chi, J.-J. Kim, Adv. Mater., 2016, **28**, 2526; (e) C. Fan, C. Yang, Chem. Soc. Rev., 2014, **43**, 6439; (f) J. Kalinowski, V. Fattori, M. Cocchi, J. A. G. Williams, Coord. Chem. Rev., 2011, **255**, 2401; (g) J. Lee, H. F. Chen, T. Batagoda, C. Coburn, P. I. Djurovich, M. E. Thompson, S. R. Forrest, Nat. Mater., 2016, **15**, 92; (h) R. McQuire, M. C. McQuire, D. R. McMillin, Coord. Chem. Rev., 2010, **254**, 2574; (i) K. S. Yook, J. Y. Lee, Adv. Mater., 2012, **24**, 3169; (j) G. E. Norby, C.-D. Park, B. O'Brien, G. Li, L. Huang, J. Li, Org. Electron., 2016, **37**, 163; (k) X.-C. Hang, T. Fleetham, E. Turner, J. Brooks, J. Li, Angew. Chem. Int. Ed., 2013, **52**, 6753.
- (a) M. A. Baldo, C. Adachi, S. R. Forrest, Phys. Rev. B: Condens. Matter Mater. Phys., 2000, **62**, 10967; (b) C.

- Murawski, K. Leo, M. C. Gather, *Adv. Mater.*, 2013, **25**, 6801; (c) Z.-Q. Zhu, K. Klimes, S. Holloway, J. Li, *Adv. Mater.*, 2017, **29**, 1605002.
- 3 (a) M. A. Baldo, S. Lamansky, P. E. Burrows, M. E. Thompson, S. R. Forrest, *Appl. Phys. Lett.*, 1999, **75**, 4; (b) M. Einzinger, T. Zhu, P. de Silva, C. Belger, T. M. Swager, T. Van Voorhis, M. A. Baldo, *Adv. Mater.*, 2017, **29**, 1701987; (c) T. Tetsuo, Y. Moon-Jae, Y. Masayuki, N. Kenji, W. Teruichi, T. Taishi, F. Yoshinori, W. Takeo, M. Satoshi, *Jpn. J. Appl. Phys.*, 1999, **38**, L1502; (d) T.-L. Wu, M.-J. Huang, C.-C. Lin, P.-Y. Huang, T.-Y. Chou, R.-W. Chen-Cheng, H.-W. Lin, R.-S. Liu, C.-H. Cheng, *Nat. Photon.*, 2018, **12**, 235.
- 4 (a) N. C. Erickson, R. J. Holmes, *Adv. Funct. Mater.*, 2013, **23**, 5190; (b) N. C. Erickson, R. J. Holmes, *Adv. Funct. Mater.*, 2014, **24**, 6074; (c) Y. Zhu, A. P. Kulkarni, P.-T. Wu, S. A. Jenekhe, *Chem. Mater.*, 2008, **20**, 4200.
- 5 (a) P. L. Burn, S. C. Lo, I. D. W. Samuel, *Adv. Mater.*, 2007, **19**, 1675; (b) S. Hecht, J. M. J. Fréchet, *Angew. Chem. Int. Ed.*, 2001, **40**, 74; (c) F. K.-W. Kong, M.-C. Tang, Y.-C. Wong, M.-Y. Chan, V. W.-W. Yam, *J. Am. Chem. Soc.*, 2016, **138**, 6281.
- 6 (a) K. Guo, H. Wang, Z. Wang, C. Si, C. Peng, G. Chen, J. Zhang, G. Wang, B. Wei, *Chem. Sci.*, 2017, **8**, 1259; (b) G. Li, Y. Feng, T. Peng, K. Ye, Y. Liu, Y. Wang, *J. Mater. Chem. C*, 2015, **3**, 1452; (c) C. Poriel, J. Rault-Berthelot, *J. Mater. Chem. C* 2017, **5**, 3869; (d) C. Tang, R. Bi, Y. Tao, F. Wang, X. Cao, S. Wang, T. Jiang, C. Zhong, H. Zhang, W. Huang, *Chem. Commun.*, 2015, **51**, 1650; (e) Z. Zhang, J. Xie, Z. Wang, B. Shen, H. Wang, M. Li, J. Zhang, J. Cao, *J. Mater. Chem. C*, 2016, **4**, 4226.
- 7 M.-C. Tang, D. P.-K. Tsang, Y.-C. Wong, M.-Y. Chan, K. M.-C. Wong, V. W.-W. Yam, *J. Am. Chem. Soc.*, 2014, **136**, 17861.
- 8 F. K.-W. Kong, M.-C. Tang, Y.-C. Wong, M. Ng, M.-Y. Chan, V. W.-W. Yam, *J. Am. Chem. Soc.*, 2017, **139**, 6351.
- 9 Q.-C. Zhang, H. Xiao, X. Zhang, L.-J. Xu, Z.-N. Chen, *Coord. Chem. Rev.*, 2018, doi.org/10.1016/j.ccr.2018.01.017.
- 10 P. S. Kuttipillai, Y. Zhao, C. J. Traverse, R. J. Staples, B. G. Levine, R. R. Lunt, *Adv. Mater.*, 2016, **28**, 320.
- 11 Y. Ma, C.-M. Che, H.-Y. Chao, X. Zhou, W.-H. Chan, J. Shen, *Adv. Mater.*, 1999, **11**, 852.
- 12 (a) J. C. Deaton, S. C. Switalski, D. Y. Kondakov, R. H. Young, T. D. Pawlik, D. J. Giesen, S. B. Harkins, A. J. M. Miller, S. F. Mickenberg, J. C. Peters, *J. Am. Chem. Soc.*, 2010, **132**, 9499; (b) D. Volz, Y. Chen, M. Wallesch, R. Liu, C. Fléchon, M. D. Zink, J. Friedrichs, H. Flügge, R. Steininger, J. Göttlicher, C. Heske, L. Weinhardt, S. Bräse, F. So, T. Baumann, *Adv. Mater.*, 2015, **27**, 2538.
- 13 T. M. Dau, Y.-A. Chen, A. J. Karttunen, E. V. Grachova, S. P. Tunik, K.-T. Lin, W.-Y. Hung, P.-T. Chou, T. A. Pakkanen, I. O. Koshevoy, *Inorg. Chem.*, 2014, **53**, 12720.
- 14 G. Cheng, G. K.-M. So, W.-P. To, Y. Chen, C.-C. Kwok, C. Ma, X. Guan, X. Chang, W.-M. Kwok, C.-M. Che, *Chem. Sci.*, 2015, **6**, 4623.
- 15 (a) B. Ma, P. I. Djurovich, S. Garon, B. Alleyne, M. E. Thompson, *Adv. Funct. Mater.*, 2006, **16**, 2438; (b) N. Su, F. Meng, J. Chen, Y. Wang, H. Tan, S. Su, W. Zhu, *Dyes Pigm.*, 2016, **128**, 68.
- 16 (a) K. Saito, Y. Hamada, H. Takahashi, T. Koshiyama, M. Kato, *Jpn. J. Appl. Phys.* 2005, **44**, L500; (b) W. Xiong, F. Meng, H. Tan, Y. Wang, P. Wang, Y. Zhang, Q. Tao, S. Su, W. Zhu, *J. Mater. Chem. C* 2016, **4**, 6007.
- 17 (a) G. Nasr, A. Guerlin, F. Dumur, L. Beouch, E. Dumas, G. Clavier, F. Miomandre, F. Goubard, D. Gimes, D. Bertin, G. Wantze, C. R. Mayer, *Chem. Commun.*, 2011, **47**, 10698; (b) Y. Zheng, A. S. Batsanov, M. A. Fox, H. A. Al-Attar, K. Abdullah, V. Jankus, M. R. Bryce, A. P. Monkman, *Angew. Chem. Int. Ed.*, 2014, **53**, 11616; (c) A. M'hamedi, M. A. Fox, A. S. Batsanov, H. A. Al-Attar, A. P. Monkman, M. R. Bryce, *J. Mater. Chem. C* 2017, **5**, 6777.
- 18 (a) X. Yang, X. Xu, J.-S. Dang, G. Zhou, C.-L. Ho, W.-Y. Wong, *Inorg. Chem.*, 2016, **55**, 1720; (b) X. Yang, Z. Feng, J. Zhao, J.-S. Dang, B. Liu, K. Zhang, G. Zhou, *ACS Appl. Mater. Interfaces*, 2016, **8**, 33874.
- 19 (a) L.-J. Xu, J.-Y. Wang, X.-F. Zhu, X.-C. Zeng, Z.-N. Chen, *Adv. Funct. Mater.*, 2015, **25**, 3033; (b) L.-J. Xu, X. Zhang, J.-Y. Wang, Z.-N. Chen, *J. Mater. Chem. C*, 2016, **4**, 1787.
- 20 (a) L.-J. Xu, X.-C. Zeng, J.-Y. Wang, L.-Y. Zhang, Y. Chi, Z.-N. Chen, *ACS Appl. Mater. Interfaces*, 2016, **8**, 20251; (b) X.-C. Zeng, J.-Y. Wang, L.-J. Xu, H.-M. Wen, Z.-N. Chen, *J. Mater. Chem. C*, 2016, **4**, 6096; (c) L.-Y. Zhang, L.-J. Xu, J.-Y. Wang, X.-C. Zeng, Z.-N. Chen, *Dalton Trans.*, 2017, **46**, 865.
- 21 (a) H.-X. Shu, J.-Y. Wang, Q.-C. Zhang, Z.-N. Chen, *Inorg. Chem.*, 2017, **56**, 9461; (b) Y.-P. Li, X.-X. Fan, Y. Wu, X.-C. Zeng, J.-Y. Wang, Q.-H. Wei, Z.-N. Chen, *J. Mater. Chem. C*, 2017, **5**, 3072.
- 22 L.-Y. Zhang, L.-J. Xu, X. Zhang, J.-Y. Wang, J. Li, Z.-N. Chen, *Inorg. Chem.* 2013, **52**, 5167.
- 23 (a) Q.-H. Wei, G.-Q. Yin, Z. Ma, L.-X. Shi, Z.-N. Chen, *Chem. Commun.*, 2003, 2188; (b) G.-Q. Yin, Q.-H. Wei, L.-Y. Zhang, Z.-N. Chen, *Organometallics*, 2006, **25**, 580.
- 24 S. Akatsu, Y. Kanematsu, T. Kurihara, S. Sueyoshi, Y. Arikawa, M. Onishi, S. Ishizaka, N. Kitamura, Y. Nakao, S. Sakaki, K. Umakoshi, *Inorg. Chem.*, 2012, **51**, 7977.
- 25 S. Yamazaki, A. J. Deeming, D. M. Speel, D. E. Hibbs, M. B. Hursthouse, K. M. A. Malik, *Chem. Commun.*, 1997, 177.
- 26 (a) J. Fornis, S. Fuertes, A. Martín, V. Sicilia, E. Lalinde, M. T. Moreno, *Chem. Eur. J.*, 2006, **12**, 8253; (b) J. P. H. Charmant, J. Fornis, J. Gómez, E. Lalinde, R. I. Merino, M. T. Moreno, A. G. Orpen, *Organometallics*, 1999, **18**, 3353; (c) B. Gil, J. Fornis, J. Gómez, E. Lalinde, A. Martín, M. T. Moreno, *Inorg. Chem.*, 2006, **45**, 7788.
- 27 T. Tanase, K. Koike, M. Uegaki, S. Hatada, K. Nakamae, B. Kure, Y. Ura, T. Nakajima, *Dalton Trans.*, 2016, **45**, 7209.
- 28 C. W. Liu, B.-J. Liaw, L.-S. Liou, J.-C. Wang, *Chem. Commun.*, 2005, 1983.
- 29 B.-J. Liaw, T. S. Lobana, Y.-W. Lin, J.-C. Wang, C. W. Liu, *Inorg. Chem.*, 2005, **44**, 9921.
- 30 Q. Wang, A. C. Marr, A. J. Blake, C. Wilson, M. Schroder, *Chem. Commun.*, 2003, 2776.
- 31 G. Fang, X. Bi, *Chem. Soc. Rev.*, 2015, **44**, 8124.
- 32 (a) H. Braunschweig, K. Radacki, R. Shang, *Chem. Sci.*, 2015, **6**, 2989; (b) C.-C. Chang, B.-S. Liao, S.-T. Liu, *Synlett*, 2007, 0283; (c) I. Krossing, I. Raabe, *Angew. Chem. Int. Ed.*, 2004, **43**, 2066; (d) C. A. Reed, *Acc. Chem. Res.*, 1998, **31**, 133.
- 33 M. T. Dau, J. R. Shkairova, A. J. Karttunen, E. V. Grachova, S. P. Tunik, A. S. Melnikov, T. A. Pakkanen, I. O. Koshevoy, *Inorg. Chem.*, 2014, **53**, 4705.
- 34 O. Munetaka, M. Jun, *Bull. Chem. Soc. Jpn.*, 2004, **77**, 953.
- 35 V. Adamovich, J. Brooks, A. Tamayo, A. M. Alexander, P. I. Djurovich, B. W. D'Andrade, C. Adachi, S. R. Forrest, M. E. Thompson, *New J. Chem.*, 2002, **26**, 1171.
- 36 (a) K. S. Yook, J. Y. Lee, *Adv. Mater.* 2014, **26**, 4218; (b) J. Liang, L. Ying, F. Huang, Y. Cao, *J. Mater. Chem. C*, 2016, **4**, 10993.
- 37 J. Guenther, J. Reibenspies, J. Blumel, *Adv. Synth. Catal.*, 2011, **353**, 443.
- 38 (a) T. Tanase, K. Koike, M. Uegaki, S. Hatada, K. Nakamae, B. Kure, Y. Ura, T. Nakajima, *Dalton Trans.*, 2016, 45, 7209; (b) M. T. Dau, J. R. Shkairova, A. J. Karttunen, E. V. Grachova, S. P. Tunik, A. S. Melnikov, T. A. Pakkanen, I. O. Koshevoy, *Inorg. Chem.*, 2014, **53**, 4705; (c) X. Zhang, J.-Y. Wang, D. Qiao, Z.-N. Chen, *J. Mater. Chem. C*, 2017, **5**, 8782.
- 39 G. M. Sheldrick, SHELXL-97, Program for the Refinement of Crystal Structures; University of Göttingen: Göttingen, Germany, 1997.

- 40 M. J. Frisch, G. W. Trucks, H. B. Schlegel, G. E. Scuseria, M. A. Robb, J. R. Cheeseman, G. Scalmani, V. Barone, B. Mennucci, G. A. Petersson, H. Nakatsuji, M. Caricato, X. Li, H. P. Hratchian, A. F. Izmaylov, J. Bloino, G. Zheng, J. L. Sonnenberg, M. Hada, M. Ehara, K. Toyota, R. Fukuda, J. Hasegawa, M. Ishida, T. Nakajima, Y. Honda, O. Kitao, H. Nakai, T. Vreven, J. A. Jr. Montgomery, J. E. Peralta, F. Ogliaro, M. Bearpark, J. J. Heyd, E. Brothers, K. N. Kudin, V. N. Staroverov, T. Keith, R. Kobayashi, J. Normand, K. Raghavachari, A. Rendell, J. C. Burant, S. S. Iyengar, J. Tomasi, M. Cossi, N. Rega, J. M. Millam, M. Klene, J. E. Knox, J. B. Cross, V. Bakken, C. Adamo, J. Jaramillo, R. Gomperts, R. E. Stratmann, O. Yazyev, A. J. Austin, R. Cammi, C. Pomelli, J. W. Ochterski, R. L. Martin, K. Morokuma, V. G. Zakrzewski, G. A. Voth, P. Salvador, J. J. Dannenberg, S. Dapprich, A. D. Daniels, O. Farkas, J. B. Foresman, J. V. Ortiz, J. Cioslowski, D. J. Fox, *Gaussian 09, revision D.01*. Gaussian, Inc., Wallingford CT, 2013.
- 41 J. P. Perdew, K. Burke, M. Ernzerhof, *Phys. Rev. Lett.* 1996, **77**, 3865.
- 42 (a) R. Bauernschmitt, R. Ahlrichs, *Chem. Phys. Lett.*, 1996, **256**, 454; (b) M. E. Casida, C. Jamorski, K. C. Casida, D. R. Salahub, *J. Chem. Phys.*, 1998, **108**, 4439; (c) R. E. Stratmann, G. E. Scuseria, M. J. Frisch, *J. Chem Phys.*, 1998, **109**, 8218.
- 43 (a) V. Barone, M. Cossi, J. Tomasi, *J. Chem. Phys.* 1997, **107**, 3210; (b) M. Cossi, G. Scalmani, N. Rega, V. Barone, *J. Chem. Phys.*, 2002, **117**, 43.
- 44 D. Andrae, U. Häussermann, M. Dolg, H. Stoll, H. Preuss, *Theor. Chim. Acta.*, 1990, **77**, 123.
- 45 P. Ros, G. C. A. Schuit, *Theo. Chim. Acta (Berl.)*, 1966, **4**, 1.
- 46 T. Lu, F. W. Chen, *J. Comp. Chem.*, 2012, **33**, 580.

**For table of contents**

Tetraphosphine-supported PtAu<sub>3</sub> cluster complexes display intense phosphorescence with quantum yields over 90% in doped films. High-efficiency solution-processable OLEDs are successfully achieved with extremely small EQE roll-off at practical brightness over 1000 cd m<sup>-2</sup>.

